

SPINEL FERRITE-HEXAFERRITE NANOCOMPOSITES: SYNTHESIS AND CHARACTERIZATION FOR HIGH FREQUENCY DEVICES FABRICATION

H. MAHMOOD^a, T. KAUSOR^a, S. LIAQAT^b, M. B. TAJ^b, M. A. MALANA^a,
M. MAHMOOD^b, M. A. YOUSUF^b, S. JABEEN^c, I. U. KHAWAJA^{d*}

^a*Institute of Chemical Sciences, Bahauddin Zakaryia University Multan, Pakistan*

^b*Department of Chemistry, The Islamia University of Bahawalpur, Pakistan*

^c*Department of Physics, Quaid-i-Azam University, Islamabad*

^d*Department of Physics, Hazara University Mansehra, KPK, Pakistan*

M-type Ca-Sr hexaferrite, spinel CoFe_2O_4 ferrite and their composites were synthesized by co-precipitation method. The structural and morphological characterization was carried out by X-ray diffraction (XRD) and electron microscopy (SEM and TEM). Their frequency dependent dielectric properties and DC resistivity measurements were carried out and discussed in detail. XRD patterns demonstrated that composites consisted of both phases i.e. hexagonal and cubic. In addition, the average crystalline size estimated from XRD data was in the range 19-38 nm. The SEM images revealed that the prepared ferrite particles are aggregated and relatively spherical in shape. DC electrical resistivity study revealed the semiconductor nature of ferrite particles and their composites. The variation of dielectric constant and dielectric loss with temperature and frequency were examined on the basis of Maxwell–Wagner model. It was observed that DC electrical resistivity of all synthesized compounds decreased with increased temperature exhibiting typical semiconductor characteristics. The activation energy obtained from temperature-dependent measurements was found in consistent with room temperature resistivity. The high value of dielectric parameters and enhanced value of resistivity suggested that the prepared materials are useful for electromagnetic attenuation and microwave devices applications.

(Received February 12, 2019; Accepted August 23, 2019)

Keywords: Spinel ferrite, Hexa ferrite, Composites, Electrical properties

1. Introduction

Nanoferrites are unique multifunctional materials having fascinating structural and electrical properties such as high surface area and low dielectric losses [1]. On the basis of crystal structure, the ferrites are categorized into two main disciplines. These disciplines are cubic ferrites and hexagonal ferrites. All cubic ferrites are spinal ferrites. Spinel ferrites are represented with general formula AB_2O_4 where A denotes divalent ions and B represents trivalent ions. Spinel ferrites have considerable importance due to vast applications i.e. magnetic cores in transformer, generators, inductors and noise suppression layers [2]. Cobalt ferrite a magnetic oxide and it is extensively used in a variety of applications i.e. gas sensors, magnetic resonance imaging, magnetic refrigerator, photo-catalyst etc. The properties of cobalt ferrite depend upon on the preparation methods, annealing temperature and raw materials. These materials have fascinated the attention of researchers in the present year attribute to the hybridized properties of composite ferrites [3]. M-type hexagonal ferrites are important materials having numerous technological applications in permanent magnets, microwave devices, high frequency devices, magnetic catalyst and magnetic recording media. Strontium hexaferrite ($\text{SrFe}_{12}\text{O}_{19}$) is a M-type hexaferrites having a hexagonal magnetoplumbite structure with space group $P63/mmc$ and is extensively studied material due to their exceptional properties such as high Curie temperature, high coercivity, very large magnetocrystalline anisotropy and high magnetization [4, 5]. The structure of M-type nanoferrites is hexagonal, in hexagon owing 64 ions for each unit cell for 11 interstices. A unit cell

* Corresponding author: kimtiaz1122@yahoo.com

is crystallized with divalent ions such as Ba^{+2} , Pb^{+2} , Sr^{+2} , 24 ferric ions and 38 oxygen ions. Fe^{3+} ions are occurred into five different voids which is elaborated as (2a, 2b, 4f1, 4f2 and 12k) as well as 3 (2a, 4f2 and 12k) site possess octahedral preference and two (2b and 4f1) having trigonal bipyramidal coordination. Ferrites properties can be tailored by controlling their composition and adopting suitable synthetic route. The literature study reveals that many efforts have been made to tailor the properties of M-type hexa-ferrites. For example *Katlakunta et al.*, [6] reported the Cr^{3+} substituted $\text{SrFe}_{12}\text{O}_{19}$ hexa-ferrites. They investigated the effect of Cr^{3+} contents on various properties of these ferrites. *Wang et al.*, [7] reported that magnetic properties of ferrites could be enhanced by substitution of transition metal cations. They studied the effect of Al^{3+} substituted with Sr-hexaferrites. The Fe^{3+} metal cations were substituted with Al^{3+} cations. This substitution resulted an increased coercivity. *Yang et al.*, [8] published a paper on Al-substituted M-type Ca-Sr hexaferrites. The magnetic properties was varied by Al substitution. The synthesis of the unsubstituted and substituted ferrite particles was carried out via ceramic technique. The results revealed that saturation magnetization (Ms) decreased, however the coercivity (Hc) increased with increased Al contents. *Ashiq et al.*, [9] studied the effect of Al-Cr doping on the structural, dielectric and magnetic properties of strontium hexaferrite nanomaterial.

To the best of our knowledge, the structural, dielectric and magnetic properties of mixed ferrite composites are rarely reported in literature. *Kotnala et al.*, [10] successfully synthesized barium ferrite and manganese nickel zinc ferrite composite using citrate gel combustion route. He found that dielectric loss decreases and the coercivity increases with the increase of hard ferrite content in the composite material. Therefore, the present study aimed at the synthesis of the M-type Ca-Sr hexaferrites ($\text{Ca}_{0.5}\text{Sr}_{0.5}\text{Fe}_{12}\text{O}_{19}$), cobalt ferrites (CoFe_2O_4) and their composites by simple and economically co-precipitation method. Furthermore, the structural, dielectric, and magnetic properties of both pure ferrites and their composites are also explored.

2. Experimental work

CoFe_2O_4 (SB), $\text{Ca}_{0.5}\text{Sr}_{0.5}\text{Fe}_{12}\text{O}_{19}$ (HB) and their composites have been synthesized by using chemical co-precipitation method. $\text{Fe}(\text{NO}_3)_3 \cdot 9\text{H}_2\text{O}$, $\text{Co}(\text{NO}_3)_2 \cdot 6\text{H}_2\text{O}$ are utilized as a starting material for synthesis. All solutions were prepared in deionized water. The appropriate amount of above solutions were mixed in a 2000 ml beaker and continuously stirred for 2h to achieve homogeneity. The temperature of magnetic hot plate was maintained upto 50-60 °C. Then, 4.0 M ammonia solution was added drop wise in the prepared solutions to attain the stable pH. For the neutralization of solution, the process of washing is done by deionized water. The synthesized precipitates were dried at 100 °C in an electric oven for overnight. A similar procedure was used for the synthesis of $\text{Ca}_{0.5}\text{Sr}_{0.5}\text{Fe}_{12}\text{O}_{19}$. The starting materials chosen were $\text{Fe}(\text{NO}_3)_3 \cdot 9\text{H}_2\text{O}$, $\text{Co}(\text{NO}_3)_2 \cdot 6\text{H}_2\text{O}$, Calcium chloride dihydrate, Strontium nitrate $\text{Sr}(\text{NO}_3)_2$ and HNO_3 . In order to attain pure phase of nanoferrites, the precipitates were annealed with the heating rate 50 °C/min in air. Pure spinel phase was obtained at 800°C for 8 hours while pure M-type ferrite was obtained at annealing temperature 950°C for 6 hours. The prepared materials CoFe_2O_4 , and $\text{Ca}_{0.5}\text{Sr}_{0.5}\text{Fe}_{12}\text{O}_{19}$ were then used to form the composites by mixing them properly in required compositions. After annealing, the synthesized ferrites and their composites were grinded in pestle mortar and packed in air tight vessels for further investigations. The unannealed powder of composites was distributed into two parts i.e. A and B. The annealing part A is carried out at 600°C for 8 hours and the annealing temperature of part B is 800°C for 8 hours to obtain mandatory cubic structure of cobalt ferrite in composites. The composites achieved at 600°C are denoted as SA-1, SA-2 and SA-3, the composites obtained at 800°C is symbolized as SB-1, SB-2 and SB-3.

3. Results and discussion

3.1. X-rays diffraction (XRD)

The phase and structural analysis of synthesized nanoferrites and their composites were confirmed by employing X-ray diffraction measurements as shown in Fig. 1. Fig. 1a and 1b shows X-ray Diffraction patterns of the parent samples and their composites at annealing temperature 600 °C and 800 °C. All the observed peaks of CoFe_2O_4 were matched well with JCPDS reference patterns 00-024-1207 while $\text{Ca}_{0.5}\text{Sr}_{0.5}\text{Fe}_{12}\text{O}_{19}$ was identified by ICSD 01-076-2496. These patterns indicated the presence of cubic and magnetoplumbite structure in cobalt and hexagonal M-type ferrites. The XRD patterns of all the nanocomposites confirmed the coexistence of both phases in the synthesized nanocomposites. Hence, the appearance of both phases confirmed the successful formation of the nanocomposites [11]. In the prepared composites, the slightly decrease in the intensity of spinel phase was observed with the increase of hexaferrite contents. It seems that the peaks of hexaferrite phase gradually dominating. The crystallite size of all the prepared compounds was calculated with the help of Scherer's formula [12]. The mathematical form of Scherer's formula is given by

$$D = k\lambda / \beta \cos \theta \quad (1)$$

Here 'k' is the shape factor and its value is 0.94, λ is wavelength of x-rays, β is full width at half maximum, and θ is Bragg's diffraction angle.

The value of average crystallite size measured from XRD data is in the range of 19-38 nm which is considerable less than the earlier reported values [13, 14]. Average crystallite size of the parent compounds and the composites annealed at 600 °C and 800 °C as a function of hexaferrite content are shown in Fig 2(a-b). It was observed that the particle size decrease by making composite of cobalt ferrite with M-hexaferrite. As reported by *Shan Che et al.*, [15], nanomaterials owing the value of crystallite size lower than 50 nm is important to acquire appropriate value of signal to noise ratio which is useful in recording media applications. In the present study, the prepared nanoferrites and their composites owing the value of crystallite size is less than 50 nm which provides good evidence of prepared samples for their application in magnetic recording media.

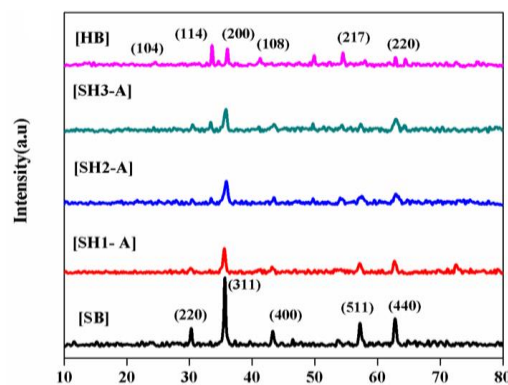


Fig. 1.a. X-ray Diffraction patterns of the parent samples and their composites SH1-A, SH2-A and SH3-A.

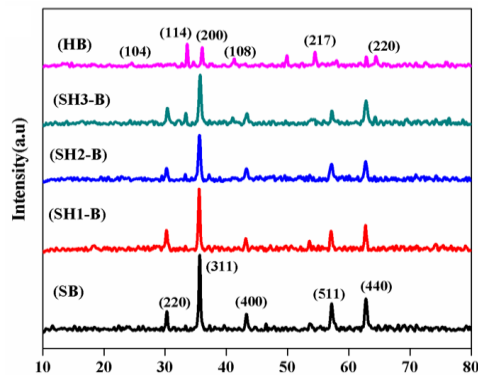


Fig. 2.b. X-ray Diffraction patterns of the parent samples and their composites SH1-B, SH2-B and SH3-B.

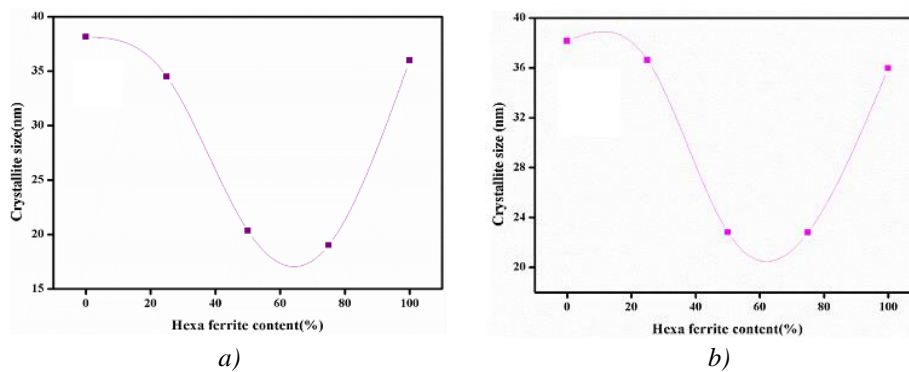


Fig. 2. Average crystallite size of the parent compounds and the composites annealed at a) 600°C and b) 800°C as a function of hexaferrite content.

3.2. Scanning electron microscopy (SEM)

The SEM micrographs of CoFe_2O_4 , $\text{Ca}_{0.5}\text{Sr}_{0.5}\text{Fe}_{12}\text{O}_{19}$ and their composites are shown in Fig. 3. These micrographs were acquired after annealing at 800 °C. Fig. 3 (a) shows that the particles of cobalt ferrites are grown in spherical form. The similar morphology of cobalt ferrite is reported by *Iqbal et al.*, [16]. The value of average particle size of cobalt ferrite obtained from SEM images comes out to be in the range 8.8 μm -38.8 μm Fig. 3 (b-d) shows the SEM images of nanocomposites. When the concentration of hexaferrites is substituted into the spinel ferrite, the cavities between the spherical particles are ornamented by worm shape large particles. Thus, heterogeneous morphology is achieved. The presence of smaller and bigger sized particles suggested the presence of both phases. All the composites possess the value of average particle size in the range 6.6 μm -32 μm . The value of average grain size of the composites decrease with the increase of hexaferrites concentration. The factor responsible for the decrease of grain size is inter particle mass transport between phases [17]. Fig. 3 (e) reveals the worm like particles of pure hexaferrite. The grain boundaries are clearly shown in pure hexaferrite and the particles are distributed in symmetric manner. The distribution of grain size of prepared hexaferrite is narrow and its value engaged in the range 8.8 μm -9.5 μm . Y. Wang et al [18] have reported the similar behavior of grain size and grain orientation. The value of average particle size investigated from SEM micrograph is greater than from the XRD measurements. It is due to the existence of nano aggregates in the composites attributed to former ones. The same behaviour has been observed by G. Asghar *et al.*, [19].

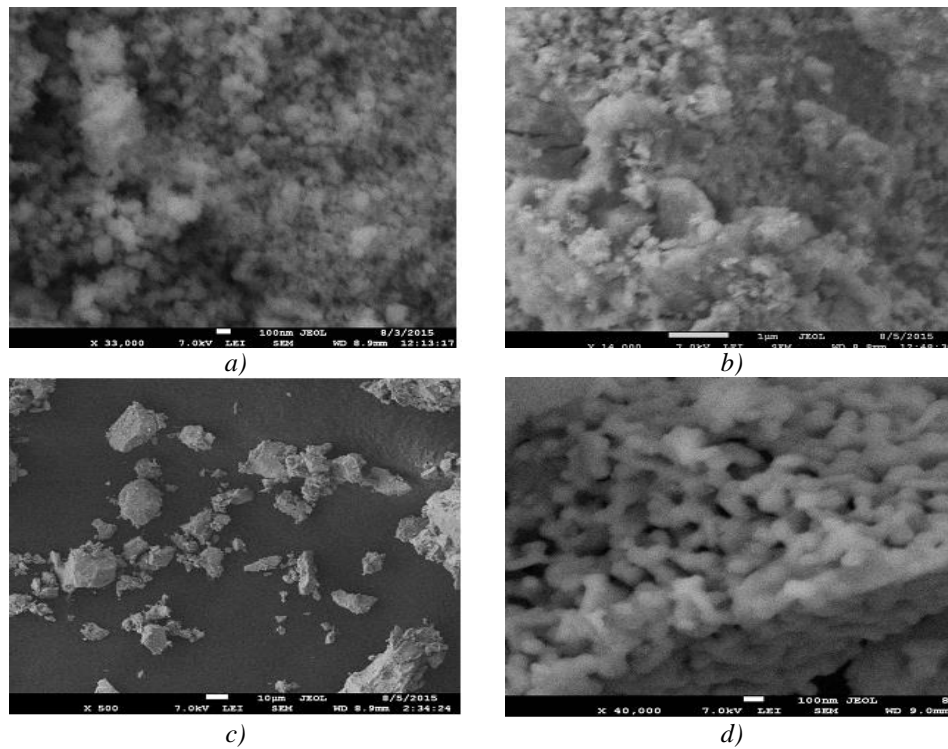


Fig. 3. SEM micrographs of a) CoFe_2O_4 ; b) composite SB-1; c) composite SB-3; d) pure Ca-Sr hexaferrite

3.3. DC electrical resistivity

DC electrical resistivity of nanomaterials was investigated in the temperature range 303-588K with the help of following equation.

$$\rho = RA / L \quad (2)$$

where, R is resistance A denotes the area and L describe pellet thickness.

Ohm's law was used to calculate the value of resistance. The equation of Ohm's law is presented below.

$$V = IR \quad (3)$$

V is voltage, I represent current and R is resistance. Fig. 4 represents the resistivity vs temperature graph of SA-1, SA-2 and SA-3 composites and SB-1, SB-2, SB-3 composites. It is clear from Fig. 4(a) and Fig. 4(b) resistivity decrease with the rise of temperature which is the characteristic of semiconductor's. Initially resistivity of hexaferrites increase with the rise of temperature and reaches upto maximum value and then decrease. The similar trend of resistivity was also observed by Yamamoto T. *et al.*, [20]. Initially increase in the value of resistivity with the rise of temperature may be attributed due to its metallic behavior. The metallic behavior contain electronic conduction due to jumping of loosely bound electrons. It is observed that transition temperature of metal to semiconductor is 518K. The value of resistivity declined at specific temperature range i.e 516-535 K. This kind of behavior in resistivity can be ascribed due to the thermally stimulated movement of charge carriers [21]. In ferrites mobility of charge carriers is affected by temperature. The concentration of charge carriers did not influenced with the temperature. The disparity in the mobility of charge is responsible for the conduction of current with the movement of electrons between Fe^{2+} - Fe^{3+} [22]. Resistivity of the nanocomposites is improved by the incorporation of hexaferrites content which is tabulated in Table 1 and 2. It is investigated that DC resistivity of samples SA-1, SA-2 and SA-3 enhance through the multiplication of ten whereas for SB-1, SB-2 and SB-3 composites is raised with the factor of hundred. The increase in resistivity was elaborated with grain size. The thin sizes of grains produce vast amount of isolating boundaries that considered as barriers for electron anticipating. Grain to grain surface region becomes small

due to smaller grain size which decrease the probability of electron hopping and increase the resistivity. Average grain size of all the synthesized composites is smaller than the pure nanoferrite which leads to increase the resistivity.

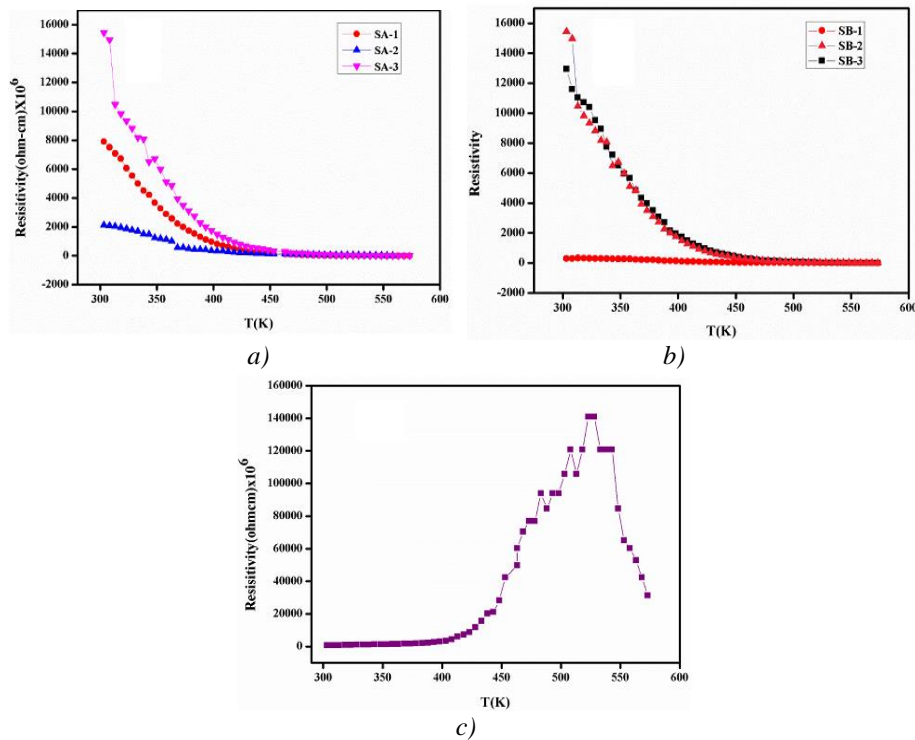


Fig. 4 DC resistivity Vs. Temperature profile of composites
a) SA-1, SA-2, SA-; b) SB-1, SB-2, SB-3; c) pure calcium strontium hexaferrite

Table 1. DC resistivities and activation energy of the parent compounds and their composites SH1-A, SH2-A, SH3-A at 303 K.

Compound	Resistivity (ohm-cm)	Ea (eV)
CoFe ₂ O ₄	1.25×10^8	0.34
Ca _{0.5} Sr _{0.5} Fe ₁₂ O ₁₉	7.96×10^8	0.88
SA-1	7.9×10^9	0.27
SA-2	2.1×10^9	0.48
SA-3	1.5×10^{10}	0.59

Table 2. DC Resistivities and activation energy of the parent compounds and their composites SH1-B, SH2-B, SH3-B at 303 K.

Compound	Resistivity (ohm-cm)	Ea (eV)
CoFe ₂ O ₄	1.25×10^8	0.34
Ca _{0.5} Sr _{0.5} Fe ₁₂ O ₁₉	7.96×10^8	0.88
SB-1	3.3×10^8	0.26
SB-2	1.4×10^{10}	0.46
SB-3	1.2×10^{10}	0.45

Equation 4 is utilized to calculate the activation energy [23, 24].

$$\ln \rho = \ln \rho^o + \frac{E_a}{K_b T} \quad (4)$$

Fig. 5 shows plot of $\ln \rho$ vs. reciprocal of temperature for prepared samples. The Table 1 and 2 shows that value of activation energy and resistivity of all the synthesized nanocomposites coordinated well with each other. The minimum energy required for the hopping of electrons is activation energy. It relies on the energy of tetrahedral and octahedral voids and space between them. Cobalt ferrite owing smaller resistivity while M-type hexaferrites possess high value of resistivity as a result the activation energy of cobalt ferrite is lower as compared to hexaferrite. All prepared samples indicated the same behavior; composites having large value of resistivity also have high E_a (activation energy).

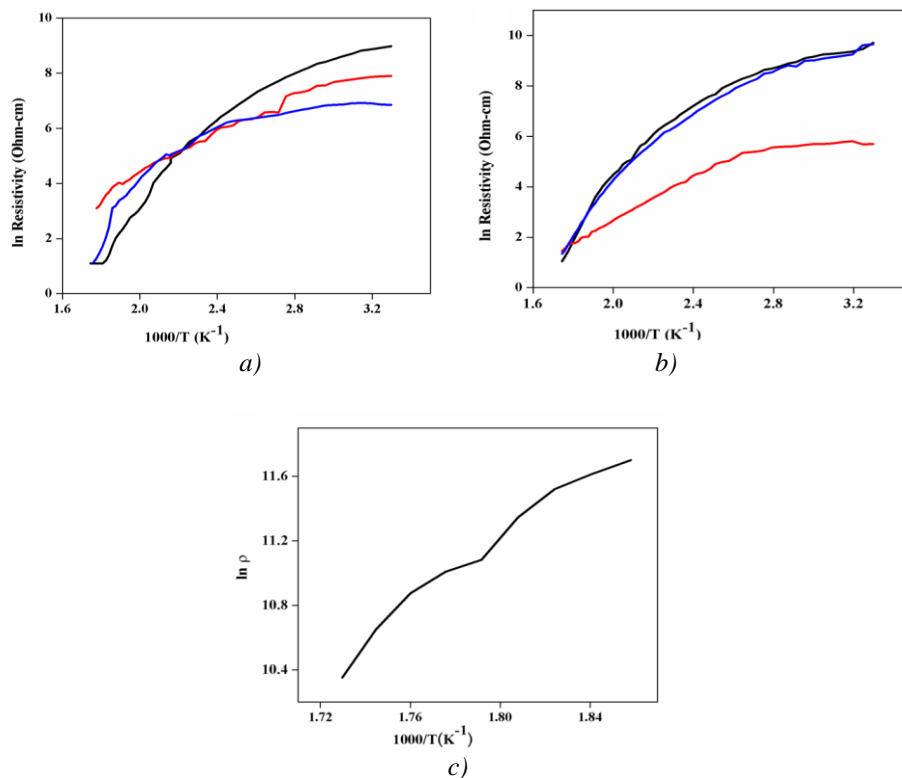


Fig. 5.a. Plot of $\ln \rho$ vs. reciprocal of temperature for SA-1, SA-2 and SA-3; b) SB-1, S-2B, and SB-3; c) pure $Ca_{0.5}Sr_{0.5}Fe_{12}O_{19}$

3.5. Dielectric properties

The dielectric constant demonstrates the relative speed of electromagnetic waves of materials. The value of real part of permittivity is essentially associated to the amount of polarization produced by the materials. Fig. 6-8 illustrates the deviation of dielectric constant, dielectric loss and tan loss for cobalt ferrites, M-type hexaferrites and their nanocomposites as a function of frequency in the frequency range 1MHz - 3 GHz at room temperature. Dielectric constant indicates sharply decreased at low frequency and became frequency independent at high frequency. This trend is general behavior of most ferrites. Space charge polarization may be responsible for the decrease in dielectric constant. The construction of ferrites and nanocomposites from grain and grain boundaries, introduced by Maxwell and Wagner is the main reason for this action [25]. The exchange of electrons between Fe^{2+} and Fe^{3+} which is the main process accumulate on the grain boundaries producing the higher values of ϵ' . But at the low frequencies, ϵ' decreases sharply with further electrons accumulations. The hopping of electrons inside the grains cannot follow up the applied frequency at high frequency; giving the independent portion.

Tan loss also found to decrease sharply at low frequencies and frequency independent at higher one. In the low frequencies, grain boundaries action exploited more energy for the transfer of electron between Fe^{2+} and Fe^{3+} , so loss is high. In the high frequencies, for the grains role little energy is needed for electrons exchange; and hence the loss is lower. The dielectric parameters of all the samples are slightly affected in the frequency 0.150 GHz to 1.80 GHz. The peaking behavior is observed in the frequency range 1.80GHz to 2.95GHz. The initial decrease in dielectric parameters with frequency has been reported by researchers [26]. At definite frequency the electronic interchange among Fe^{2+} - Fe^{3+} ions equal to the external electric field frequency. Hence peaking behavior preserve all the synthesized nanoferrites and their composites. Resonance peaks attained at 1.81-1.89 GHz and 2.46 - 2.58 GHz for all the samples. First peak was ascribed due to interfacial polarization. While second peak observed is due to ionic relaxation. In the present studies dielectric constant exhibited small values at higher frequency which may suggest that prepared composites are suitable for microwave devices at higher frequencies region [27].

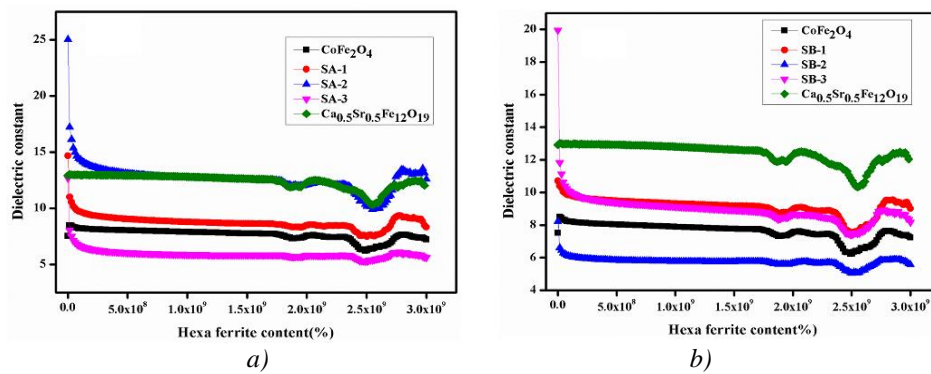


Fig. 6.a. Frequency dependent dielectric constant for the cobalt ferrites, Ca-Sr hexaferrites and their composites annealed at a) 600 °C; b) 800 °C.

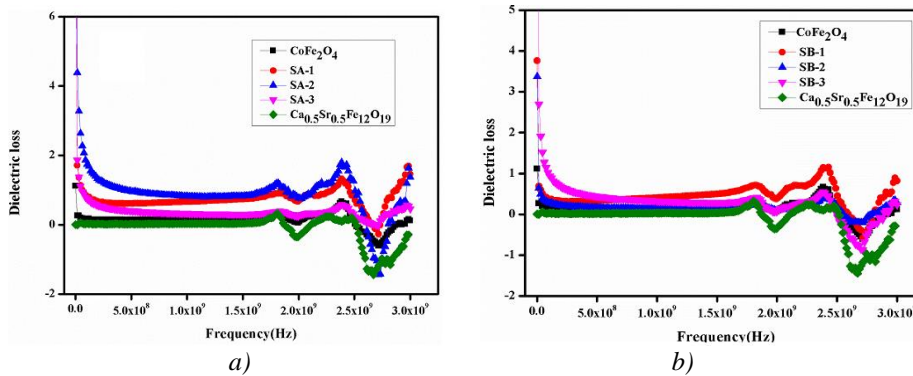


Fig. 7. Frequency dependent dielectric loss for the cobalt ferrites, Ca-Sr hexaferrites and their composites annealed at a) 600 °C; b) 800 °C.

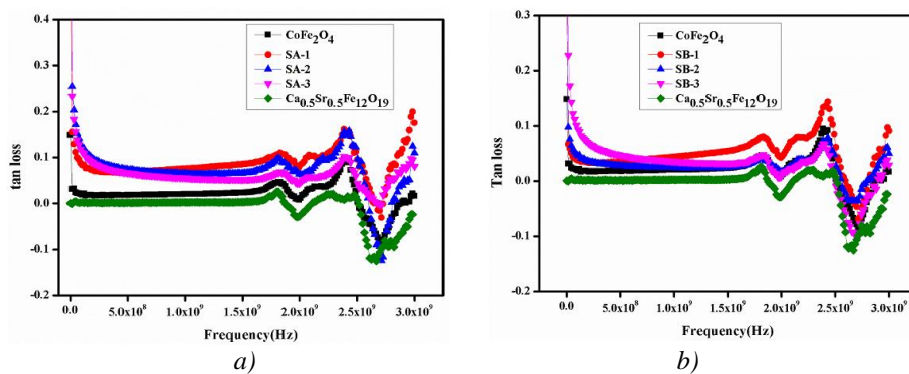


Fig. 8 Frequency dependent tan loss for the cobalt ferrites, Ca-Sr hexaferrites and their composites annealed at a) 600 °C; b) 800 °C.

The ac conductivity of all the prepared materials was measured at room temperature and shown in Fig. 9. Equation 5 was used to investigate the ac conductivity

$$\sigma_{ac} = \omega \epsilon_0 \epsilon' \tan \delta \quad (5)$$

The ac conductivity introduces an increasing behavior with frequency. It is observed that AC conductivity increase slowly with the increase in frequency [28]. The electrons migration under the frequency of the applied field is contributing to the electrical restraint of the ferrite. The ac conductivity due to hopping technique is an increasing function of the applied frequency. This behavior explained by Maxwell Wagner model [25]. The conductive layer is activating with the increase of frequency which enhance the hopping of electron between Fe²⁺-Fe³⁺ ions. Conductivity is increased due to enhance of hopping.

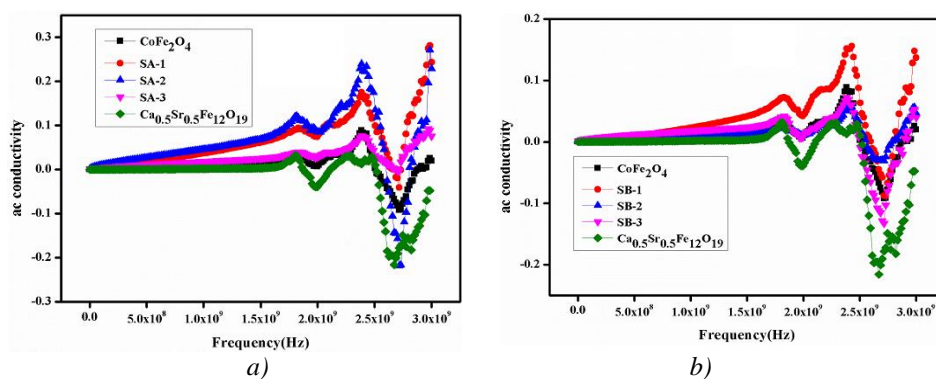


Fig. 9 Frequency dependent ac conductivity of the cobalt ferrites, Ca-Sr hexaferrites and their composites annealed at a) 600 °C; b) 800 °C.

4. Conclusions

In this study, co precipitation method has been employed for the synthesis of M-type Ca-Sr hexaferrite, CoFe₂O₄ and their composites. XRD spectra confirmed the cubic structure of cobalt ferrite with the lattice parameter $a = 8.36 \text{ \AA}$ and hexagonal structure of Ca-Sr ferrite with the lattice parameters $a = 12.99 \text{ \AA}$, $c = 23.19 \text{ \AA}$. XRD patterns of mixed ferrites demonstrated the characteristic peaks of both ferrites showing the coexistence of both the phases in composite material. The particle size measured from XRD, SEM and TEM techniques confirmed the nanocrystalline size of prepared samples. For all the samples, the dielectric loss and tangent loss showed normal behavior of dielectric with frequency.

The activation energy and resistivity plots exhibited similar behavior which shows that the samples with high resistivity have high activation energy. The high value of the dielectric constant and enhanced resistivity of the composites, recommends them suitable candidates for microwave absorption devices.

References

- [1] C. N. R. Rao, K. Gopalakrishnan, U. Maitra, *ACS Applied Materials & Interfaces* **7**, 7809 (2015).
- [2] N. Y. Lanje, D. K. Kulkarni, *Journal of Magnetism and Magnetic Materials* **234**, 114 (2001).
- [3] M. U. Islam, F. Aen, S. B. Niazi, M. Azhar Khan, M. Ishaque, T. Abbas, M. U. Rana, *Materials Chemistry and Physics*, **109**, 482 (2008).
- [4] S. Ashima, A. Sanghi, Reetu Agarwal, *Journal of Alloys and Compounds* **513**, 436 (2012).
- [5] R. Alange, P. P. Khirade, S. D. Birajdar, K. Jadhav, *Journal of Materials Science: Materials in Electronics* **28**, 407 (2017).
- [6] S. Katlakunta, S. S. Meena, S. Srinath, M. Bououdina, R. Sandhya, K. Praveena, *Materials Research Bulletin* **63**, 58 (2015).
- [7] H. Wang, B. Yao, Y. Xu, Q. He, G. Wen, S. Long, J. Fan, G. Li, L. Shan, B. Liu, *Journal of Alloys and Compounds* **537**, 43 (2012).
- [8] Y. Yang, F. Wang, X. Liu, J. Shao, D. Huang, *Journal of Magnetism and Magnetic Materials* **421**, 349 (2017).
- [9] M. N. Ashiq, M. J. Iqbal, I. H. Gul, *Journal of Magnetism and magnetic materials* **323**, 259 (2011).
- [10] R. Kotnala, S. Ahmad, A. S. Ahmed, J. Shah, A. Azam, *Journal of Applied Physics* **112**, 054323 (2012).
- [11] W. Qu, X. Wang, L. Li, *Materials Science and Engineering: B* **99**, 274 (2003).
- [12] H. Malik, M. A. Khan, A. Hussain, M. F. Warsi, A. Mahmood, S. M. Ramay, *Ceramics International* **44**, 605 (2018).
- [13] M. M. Rashad, M. Radwan, M. M. Hessien, *Journal of Alloys and Compounds* **453**, 304 (2008).
- [14] M. N. A. Muhammad Javed Iqbal, Iftikhar Hussain Gul Changrui, Zhang, *Journal of Magnetism and Magnetic Materials* **322**, 1720 (2010).
- [15] Shan Che, Jun Wang, Q. Chen, *Journal of physics:condensed matter* **15**, 335 (2003).
- [16] M. J. Iqbal, S. Farooq, *Materials Research Bulletin* **44**, 2050 (2009).
- [17] H. Zhang, L. Li, Z. Ma, J. Zhou, Z. Yue, Z. Gui, *Journal of Magnetism and Magnetic Materials* **218**, 67 (2000).
- [18] Y. Wang, L. Li, H. Liu, H. Qiu, F. Xu, *Materials Letters* **62**, 2060 (2008).
- [19] G. Asghar, M. Anis-ur-Rehman, *Journal of Alloys and Compounds* **526**, 85(2012).
- [20] T. Yamamoto, R. Kanno, Y. Takeda, O. Yamamoto, Y. Kawamoto, M. Takano, *Journal of Solid State Chemistry* **109**, 372 (1994).
- [21] M. J. Iqbal, Z. Ahmad, *J. Power Sources* **179**, 763 (2008).
- [22] E. Rezlescu, L. Sachelarie, P. D. Popa, N. Rezlescu, *IEEE Transactions on Magnetism* **36**, 3962 (2000).
- [23] M. N. Ashiq, S. Saleem, M. A. Malana, R. Anis Ur, *Journal of Alloys and Compounds* **486**, 640 (2009).
- [24] T. Abbas, M. U. Islam, M. Ashraf Ch, *Modern Physics Letters B* **09**,1419 (1995).
- [25] C. G. Koops, *Physical Review* **83**, 121(1951).
- [26] M. Iqbal, R. Khan, *Journal of Alloys and Compounds* **478**, 847 (2009).
- [27] M. J. Iqbal, R. A. Khan, S. Mizukami, T. Miyazaki, *Journal of Magnetism and Magnetic Materials* **323**, 2137(2011).
- [28] M. N. Ashiq, R. B. Qureshi, M. A. Malana, M. F. Ehsan, *Journal of Alloys and Compounds* **617**, 437(2014).